ACS APPLIED MATERIALS & INTERFACES

Research Article

Cite This: ACS Appl. Mater. Interfaces XXXX, XXX, XXX−XXX

www.acsami.org

Electrides with Dinitrogen Ligands

Jingyu Qu,[†,‡] Shengcai Zhu,[‡] Weiwei Zhang,*[,†] and Qiang Zhu*[,‡]

[†]College of Science, China Agricultural University, Beijing 100083, China

[‡]Department of Physics and Astronomy, High Pressure Science and Engineering Center, University of Nevada, Las Vegas, Las Vegas, Nevada 89154, United States

Supporting Information

ABSTRACT: Electrides are a class of materials which contain excess electrons occupying the cavities in the crystal and playing the role of anions. To achieve electron-rich conditions, it usually requires a positive total formal charge in electride materials. However, the assignment of charges relies on a detailed analysis on chemical bonding. Herein, we present a survey on potential electrides which may be overlooked if no bonding analysis is performed. By applying various structure sampling techniques in conjunction with first-principles calculation, we predicted two compounds Ba_2N_2:e^- and $Li_2Ca_3N_6$:$2e^-$, both of which are featured by the presence of dinitrogen ligands $[N_2]$, to be potential electrides. While $Li_2Ca_3N_6$:$2e^-$ with $[N_2]^{2-}$ ions has been synthesized in the past, its electride nature was discovered for the first time based on our high-throughput screening. On the other hand, Ba_2N_2:e^- with $[N_2]^{3-}$ ions is a new compound entirely from first-principles structure prediction. The different valence states of dinitrogen ligands identified in these two compounds suggest a novel route to tune the concentration and anisotropic properties of anionic interstitial electrons. Our discovery does not only establish a new class of inorganic electrides but also demonstrates the predictive power of modern crystal structure sampling techniques toward rational material design.

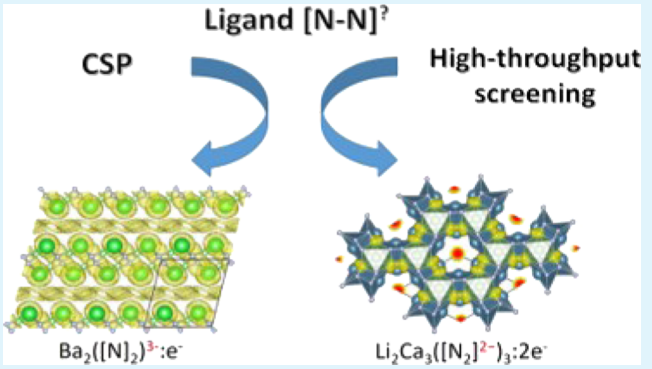

KEYWORDS: *electride, high-throughput calculation, crystal structure prediction, catalysis, polyatomic anions*

INTRODUCTION

Electrides are crystalline solids with excess electrons occupying the crystal cavities. These interstitial electrons behave as anions instead of attaching to any atoms.[1,2] According to the distribution of anionic electrons, electrides can be classified by dimensionality from zero to one and two dimensions. The first electride was discovered in the organic material $Cs^+(15\text{-crown-}5)_2$:$e^-$ by Dye and co-workers.[3] Organic electrides are unstable at room temperature, which limits their practical application.[1] The synthesis of inorganic electrides has drawn growing attention because of their promise in higher thermal stability and less chemical sensitivity relative to their organic counterpart. The first inorganic electride was experimentally realized in $C_{12}A_7$:$2e^-$,[4] which has been proved to show good performance for the application of a catalyst[5,6] and an electron field emitter.[7] Moreover, Ca_2N, originally synthesized in 1966,[8] was found to be the first example of a two-dimensional (2D) electride by Lee et al. until recently.[9] Because of the strong anisotropic character, 2D electrides exhibit many appealing properties, such as low work function,[9,10] high electron mobility,[11] and so forth, which are advantageous for applications in the anode material of batteries[12] and cathodes of polymer light-emitting diodes[13] and photonic devices.[14] These great promises have stimulated a number of experimental efforts in searching for new candidates of electride materials.[15−20]

Parallel to the growing efforts in experiments, material design based on first-principles calculations has been playing an increasingly important role in the discovery of new electrides.[21−24] On the basis of the Ca_2N prototype, a series of 2D electrides have been proposed.[21,22] On the other hand, the recent advances in crystal structure prediction (CSP) made it possible to search for new materials with unknown structure prototypes.[17,23,24] For example, Zhang et al.[24] proposed an inverse design strategy to search for inorganic electrides. Using the interstitial electron's electron localization function (ELF) as the optimization target, they identified a number of potential electrides A_2B and AB compounds. Furthermore, Wang et al.[17] pointed out that one had to consider the possibility of competing phases with different stoichiometries in the crystal structure search. By applying the variable compositional structure search to the Sr−P system, they found two new stable electrides Sr_8P_5 and Sr_5P_3. However, such first-principles CSP is computationally expensive, and thus, the applications

Received: October 24, 2018
Accepted: January 15, 2019
Published: January 15, 2019

DOI: 10.1021/acsami.8b18676
ACS Appl. Mater. Interfaces XXXX, XXX, XXX−XXX

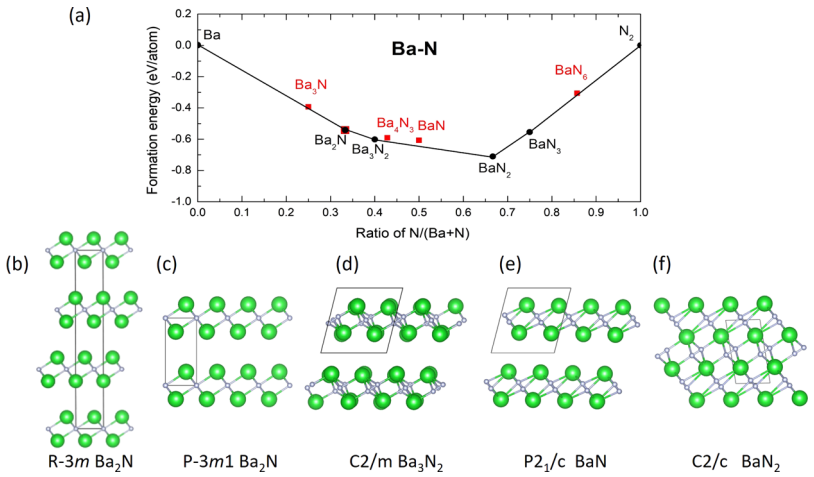

Figure 1. (a) Convex hull diagram of the Ba−N system at the optB86b level. In the diagram, the red squares denote metastable compounds and black circles represent stable compounds. Some representative structures discussed in this work are shown in (b) $R\bar{3}m$ Ba_2N, (c) $P\bar{3}m1$ Ba_2N, (d) Ba_3N_2, (e) BaN, and (f) BaN_2. The large green spheres represent Ba atoms, while the small silver spheres represent N atoms.

were limited to a small set of chemical systems. It is highly likely that the electride materials are far underexploited. Our understanding on the electride remains limited by the relatively small number of known electride materials.

Toward the goal of finding new electrides, various computational screening strategies have been proposed, including the positive total formal charge, significant crystal voids, strong non-nuclear electron localization, and so forth.[21,24−26] Among them, stoichiometry analysis has been widely used for the very first step of screening, as it assumes that the ideal electride at ambient conditions must possess positive total formal charges to form the anionic electrons.[21] However, the charge assignment requires a detailed analysis on the chemical bonding, as atoms in different chemical environments may adopt different valence states. Recently, Burton et al.[26] performed a large-scale computational screening for electrides among known materials in Materials Project database.[27] They inspected projections on atomic orbitals and Bader charge instead of any previous design principles such as excess electrons from oxidation state estimation. Sixty five new electride candidates were reported, plenty of which do not follow the rule that excess electrons exist in the sum of oxidation states. This suggests that there may exist some exceptional electrides in which the atoms adopt less common valence states in the conventional ionic solids.

In this work, we combined first-principles evolutionary CSP[28,29] with high-throughput screening methods (from the online database of Materials Project[27]) based on density functional theory (DFT), which allows us to effectively explore the structural space with unknown structural prototypes and calculate their stability maps in a variety of chemical systems. Interestingly, we identified a new electride BaN with an unexpected stoichiometry featured by the presence of dinitrogen ligands. This further motivated us to perform an extended search on possible electride materials which may possess a $[N_2]$ unit. We indeed found another compound $Li_2Ca_3N_6$ from the existing material database as the potential inorganic electride. Our detailed charge analysis revealed that the $[N_2]$ units in these two materials possess different valence states. This discovery suggests a new class of electrides which exhibit different stoichiometries and perhaps physical properties as well.

COMPUTATIONAL METHODS

Crystal Structure Search. We adopted two strategies to search for the candidate crystal structures which are potential electrides, including first-principles CSP and material screening from the available database. First, we investigated several alkaline metal nitride systems by using the evolutionary structure prediction code USPEX,[28,29] with the goal of finding new electrides beyond the well-known Ca_2N prototype.[9] To enable this, we have recently employed the variable composition prediction function to search for possible thermodynamically stable compounds within Ca−N, Sr−N, Ba−N, and many other relevant systems.[30] During our search, we restricted the maximum number of atoms to 24. USPEX adopts the idea of self-learning by mimicking the biological evolution in mother nature.[31] The initial structures are constructed randomly at the first generation, followed by geometry optimization and energy ranking. For the following generations, low-energy structures are selected based on the tournament selection rule to produce new populations by different variation operators such as heredity, mutation, and permutation. According to our past experience, an empirical setting for the fraction of each variation operation is 30% (heredity), 30% (random), 20% (mutation), and 20% (permutation). We terminated the search for each run until 40 generations, which is usually sufficient for the exploration of binary compounds.

In addition to the first-principles CSP, we took advantage of the existing computational material database of Materials Project.[27] We developed a scheme to systematically search for structures containing structural units like $[N_2]$ and $[C_2]$. From the entire database, we identified 142 structures containing $[N_2]$ ligands. A subsequent analysis on their electronic structures finally identified that $Li_2Ca_3N_6$ is an electride with pernitride anions.

DFT Calculation. For each generated structure either from first-principles CSP or database screening, we carried out DFT calculations using the all-electron projector wave (PAW) method[32] implemented in the VASP code.[33] The exchange−correlation energy was treated within the generalized gradient approximation using the functional of Perdew, Burke, and Ernzerhof.[34] Van der Waals (vdW) interactions were described by the optB86b-vdW functional.[35] The plane-wave cutoff energy is set to be 800 eV, and a Γ-centered Brillouin zone sampling grid with KSPACING = 0.16 is chosen. The convergence threshold is 10^{-8} eV to ensure that all calculations are well-converged, and all structures were relaxed until the forces on the atoms became smaller than 0.001 eV/atom. To compare the relative stability of the compounds with different compositions, we plotted the convex hull diagram. Because all the stable Ba_xN_y structures should not decompose into any other counterpart, they form the based convex hull in the normalized formation enthalpy versus composition map, while the relative stability of any other unstable compound can be

DOI: 10.1021/acsami.8b18676
ACS Appl. Mater. Interfaces XXXX, XXX, XXX−XXX

measured by its vertical distance to the hull. The dynamic stability of the structures was carefully checked by the phonon spectra calculation with the finite displacement method as implemented in the Phonopy code.[36]

To characterize the electride property for a given material, we performed several steps of calculations based on different criteria. First, we computed the ELF and looked for the existence of the ELF maxima which do not belong to either core electrons around ions or electrons shared by covalent bonds.[24] Second, we placed pseudoatoms on these interstitial ELF maxima with certain Wigner−Seitz radii and computed the projected portions of the wave function within these spheres to obtain the density of states (DOS) for the interstitial electrons. The appropriate Wigner−Seitz radii of the interstitial electrons were chosen based on the size of interstitial space, which is typically between 1.8 and 2.5 Å.[9,17] The electronic band structures were calculated by following the *K* point path according to a previous literature study.[37] Third, we analyzed the projected partial charge density for each energy band near the Fermi level to check if they possess interstitial electrons. Subsequently, the energy range from the lower limit of the interstitial bands to the Fermi level was selected to perform the Bader charge analysis[38] by inserting the psesudoatoms to the same positions. Last, we computed the occupation of the interstitial electrons on each energy band based on the projection by considering the ratio of DOS projected to each ion. In such a band structure calculation, the Wigner−Seitz radii for different ions were set based on the values suggested in the corresponding POTCAR files from the VASP code.

RESULTS AND DISCUSSION

BaN from First-Principles Structure Prediction. Our searches on Ca−N, Sr−N and Ba−N at ambient conditions yield a number of interesting low-energy structures with different compositions. However, we highlight our results on Ba−N binary (shown in Figure 1), as this is the only system which yields a totally new compound close to be thermodynamically stable. On the basis of our calculation with vdW correction, we determined that Ba_2N, Ba_3N_2, BaN_2, and BaN_3 are stable, while Ba_3N, Ba_4N_3, BaN, and BaN_6 are marginally stable (<34.9 meV/atom). The corresponding structure details are available in the Supporting Information. Ba_3N, Ba_2N, BaN_6, and BaN_2 have been reported experimentally.[39−43] This validated our structure prediction approach used here. Among these known materials, several barium-rich compounds Ba_3N_2, Ba_3N, and Ba_2N have been proposed to be electrides.[44,45] Notably, we identified several new low-energy forms of Ba_2N, in addition to the well-known $R\bar{3}m$ $CaCl_2$ type. In particular, the structure with $P\bar{3}m1$ symmetry (Figure 1c) is very similar to the $R\bar{3}m$ structure (Figure 1b), while it only differs in the stacking sequence. The formation energy of $P\bar{3}m1$ Ba_2N is 1.6 meV/atom lower than $R\bar{3}m$ Ba_2N. More interestingly, we also found a few new structures with other stoichiometries. Among them, we highlight the unique compound BaN, which is only about 34.9 meV/atom above the convex hull. As we will discuss in the following section, BaN, though looking like a nitrogen-rich compound, is actually an electride.

Very recently, Huang and Frapper also adopted a similar evolutionary structure prediction in Ba−N systems.[45] The comparison between our work and Huang's results is summarized in the Supporting Information (Table S1). We found that the $C2/m$-Ba_3N_2 (Figure 1d) in their paper has a slightly lower formation energy. This structure has been added to our convex hull diagram as well, but it leads to only a little change in the convex hull.

As shown in Figure 1e, BaN possesses a layered structure in monoclinic $P2_1/c$ symmetry with four formula units in the conventional cell. The detailed crystallographic information is listed in Table 1. Similar to Ba_2N, BaN has a layered structure.

Table 1. Crystallographic Data of BaN[a]

atom	Wyckoff	coordinates	charge (|e|/atom)
Ba	4e	(0.208, 0.566, 0.250)	1.540
N	4e	(0.051, 0.108, 0.050)	−1.201
X	2d	(0.500, 0.000, 0.500)	−0.678

[a]It crystallizes in the space group $P2_1/c$ with the cell parameters of a = 7.79 Å, b = 4.25 Å, c = 7.26 Å, and β = 104.11°. The detailed atomic coordinates are shown in the table.

However, each two N atoms are paired together, unlike each N in Ba_2N (Figure 1b,c), playing the role of anions. The presence of $[N_2]$ units reduces the symmetry from rhombohedral to monoclinic class. In addition, $C2/m$-Ba_3N_2 (Figure 1d) also has a layered structure, in which the N atoms have mixed bonding states resembling those in BaN and Ba_2N. Both Ba_2N[21] and Ba_3N_2[45] were suggested to possess interstitial electrons between the layers. Given their strong similarity between BaN, Ba_3N_2, and Ba_2N, it is natural to speculate that BaN may be also an electride.

To verify this hypothesis, we calculated the ELF as shown in Figure 2a−c. Both the isosurface (η = 0.35) and sliced map plots unambiguously reveal that there exist ELF maxima (denoted as X from now on) between two adjacent layers. We did not find any other basin along the path from X to other ELF maxima, suggesting that the interactions are ionic. In addition to the anionic X sites, another type of prominent ELF maxima appears around the N−N bond, as shown in Figure 2c. There exist ELF maxima in both the N−N center and N−N dumbell, suggesting a mixed bonding in the $[N_2]$ entity, namely, the covalent bond between N−N and the ionic bonding between $[N_2]$ and others. The existence of interstitial electrons around the Fermi level is usually considered to be the main character for an electride. To check the energy distribution of the X sites, we computed the decomposed partial charge density around the Fermi level (-1 eV < $E - E_{Fermi}$< 0 eV). Notably, the DOS around the Fermi level is primarily contributed by two sources: (1) the $[N_2]$ units and (2) the electron cloud between the layers, indicating the electride nature of BaN. This was further supported by our electronic band structure and DOS plots as shown in Figure 3a,b. By probing the partial charge density for each band close to the Fermi level, we identified that several bands (marked as red in Figure 3a) are attributed to the localized electrons between the layers. Clearly, our detailed electronic structure analysis confirmed that BaN is an electride.

Because both BaN and Ba_2N are electrides with very similar crystal packing, it would be interesting to know how diatomic $[N_2]$ in BaN differs from monoatomic N in BaN_2. The $[N_2]$ ligand has been known to adopt various coordination environments and valence states.[46] An empirical way to estimate its valence state is via the N−N bond length. The N−N distance in BaN is 1.31 Å, which is roughly between the range of $[N_2]^{2-}$ (1.230−1.318 Å)[47,48] and $[N_2]^{3-}$ (1.396−1.402 Å).[49] This gives us the first estimation that the valence state of each $[N_2]$ unit in BaN should be either -II or -III. By analyzing the projected Ba and N DOS in Figure 2b, we found that the DOS around the Fermi level is primarily contributed

DOI: 10.1021/acsami.8b18676
ACS Appl. Mater. Interfaces XXXX, XXX, XXX−XXX

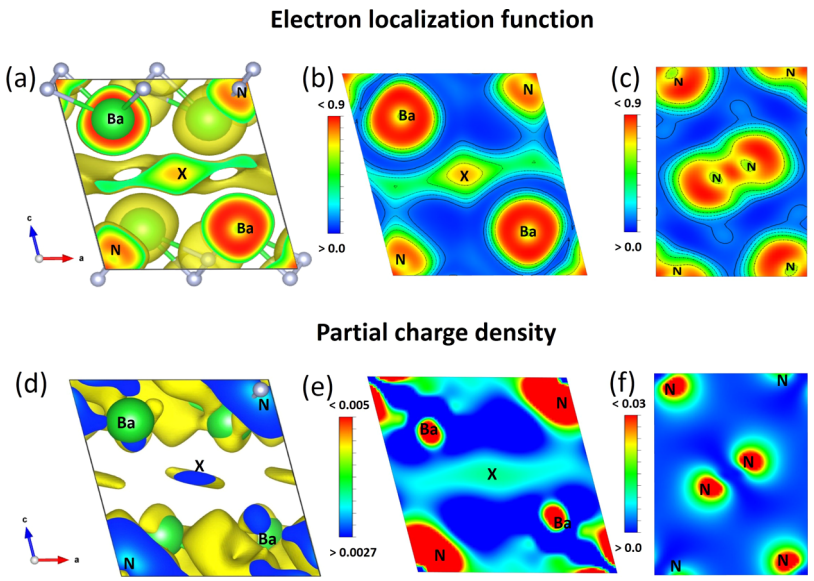

Figure 2. Electronic structure analysis of BaN. (a) Isosurface plot of ELF at η = 0.35; the corresponding sliced 2D map of (010) plane (b) and (001) plane (c); (d) the isosurface plot of the partial charge density at 0.0035 e/Å^{-3} around the Fermi level (-1 eV < $E - E_{Fermi}$< 0 eV); and the corresponding 2D charge density map of (010) plane (e) and (001) plane (f).

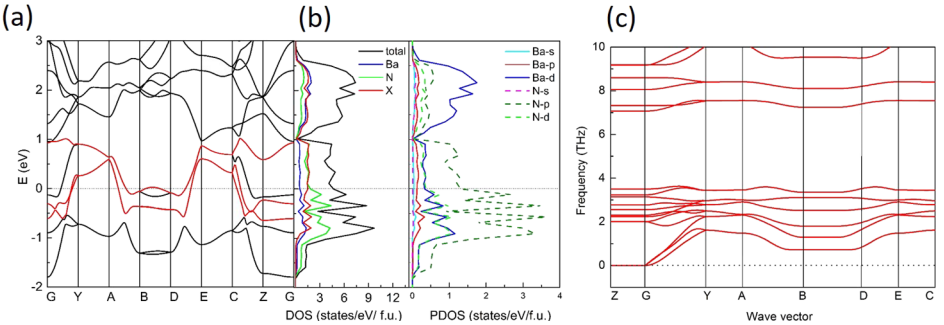

Figure 3. (a) Calculated band structure and (b) projected DOS of BaN and (c) phonon dispersion curves of BaN.

by N 2p and Ba 5d. The overlap between N 2p and Ba 5d indicates an interaction between Ba and $[N_2]$, which was suggested to be the possible cause of a smaller N−N bond length than that in a typical N−N single bond (1.45 Å).[45] To obtain more physical insights, we also performed a Bader charge analysis[38] by following a numerical approach described in the previous literature.[50] Bader charge analysis exploits the topological properties of the charge density and partitions the space into several subsystems. Each volume of the subsystem is assigned to the nearest nucleus. The boundary of the charge basin is determined by the zero-flux charge density gradient between the nucleus. To correctly capture the charge distribution, we again inserted the X sites as the artificial nucleus in the calculation. In BaN, the Bader partition yielded three primary charge basins, Ba (1.540e), $[N_2]$ ($-2.402e$), and X ($-0.678e$). For the reference, we found that the results in Ba_2N are Ba (1.229e), N ($-1.757e$), and X ($-0.695e$). Clearly, Ba atoms in BaN tend to lose more electrons, and the extra charges go to the $[N_2]$ sites, suggesting that $[N_2]$ in BaN is more electronegative than N in Ba_2N, which is consistent with our prior projected DOS analysis on the N 2p and Ba 5d orbital overlap. On the other hand, the charges on interstitial sites remain consistent between BaN and Ba_2N. Thus, each interstitial site in BaN should possess the same number of extra electrons as its counterpart layered form $Ba_2N{:}e^-$. The corresponding formula of BaN should be $Ba_2[N_2]{:}e^-$. In this sense, we conclude that $[N_2]$ in BaN is more likely to exhibit -III state.

Last, we checked the dynamic stability of BaN by phonon calculation. Indeed, there is no imaginary frequency in the phonon spectrum in the whole Brillouin zone (see Figure 3c). Thus, BaN can survive at ambient conditions if it can be synthesized. Indeed, several stable compounds with polynitride anions have been reported in the Ba−N system, including BaN_2 and BaN_6. In particular, BaN_2 (Figure 1e), which is adjacent to BaN in the convex hull diagram (Figure 1a), has been synthesized by controlling of decomposition of the corresponding azide under high temperature and high pressure.[51] Therefore, a possible synthetic route of BaN is to mix BaN_2 with Ba by using BaN_2 as the precursor of $[N_2]$.

$Li_2Ca_3N_6$ from High-Throughput Screening. The identification of BaN as the first example of an electride with $[N_2]$ ligands is somewhat unexpected. Because the previous screening mostly focused on the structures which apparently have positive formal charges, it is likely that such materials like BaN were overlooked in the past. Therefore, we further performed an extended search for materials consisting of $[N_2]$ ligands in the Materials Project database, from which we obtained 142 candidate structures. By carefully examining their

DOI: 10.1021/acsami.8b18676
ACS Appl. Mater. Interfaces XXXX, XXX, XXX−XXX

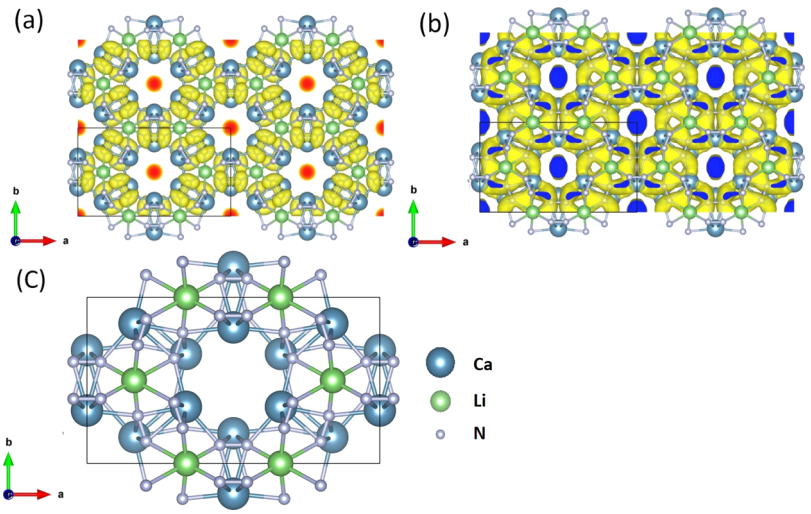

Figure 4. (a) Isosurface of ELF in $Li_2Ca_3N_6$ at $\eta = 0.7$; (b) isosurface of the partial charge density for states between $E_{Fermi} \pm 0.025$ eV at 0.00045 e/Å^{-3}; and (c) atomic structure of $Li_2Ca_3N_6$ in the conventional unit cell.

partial charge density distribution near the Fermi level, we finally identified another new electride $Li_2Ca_3N_6$.

$Li_2Ca_3N_6$ is the first ternary compound with homonuclear dinitrogen reported in the literature.[52] This material was synthesized under high temperature and high pressure by controlling thermal decomposition of the mixing ratio of ionic lithium and calcium azides.[52] Its crystal structure was originally determined to have an orthorhombic Bravis cell with *Pmma* symmetry (no. 51). However, we found that the further geometry relaxation from the experimentally resolved structure led to a base-centered cell with *Cmcm* symmetry (no. 63), as shown in Figure 4c. Nevertheless, the differences between two structures are nearly negligible. For the sake of consistency, we used the *Cmcm* structure (see details in Table 2) in our study.

Table 2. Crystallographic Data of $Li_2Ca_3N_6$[a]

atom	Wyckoff	coordinates	charge (|e|/atom)
Li_1	8f	(0.167, 0.500, 0.000)	1.000
Ca_1	8g	(0.160, 0.160, 0.250)	1.450
Ca_2	4c	(0.000, 0.319, 0.750)	1.974
N_1	8g	(0.047, 0.391, 0.250)	−1.017
N_2	8g	(0.174, 0.273, 0.750)	−1.022
N_3	8g	(0.216, 0.128, 0.750)	−1.008
X	4a	(0.000, 0.000, 0.000)	−0.560

[a]It crystallizes in the space group *Cmcm* with the conventional cell parameters of $a = 14.03$ Å, $b = 8.07$ Å, and $c = 4.75$ Å. The detailed atomic coordinates are shown in the table.

The conventional cell of $Li_2Ca_3N_6$ contains 12 nitrogen dimers, each of them is octahedrally coordinated by 4 calcium and 2 lithium cations. Such a coordination environment is similar to that in the electron-rich suboxides: Rb_6O and Rb_9O_2.[52] Though the $[N_2]$ ligand in $Li_2Ca_3N_6$ has a similar N−N bond length (1.31 Å) with that in BaN, the previous work suggested that the $[N_2]$ entity exhibits -II valence state (instead of -III), based on a variety of experimental techniques and DFT calculations.[52] Following this valence rule, $(Li^+)_2(Ca^{2+})_3([N_2]^{2-})_3{:}2e^-$ was considered to be an electron-rich compound with two extra electrons per unit.

However, a compound with electron-rich conditions is not necessarily an electride. The ELF isosurface of $Li_2Ca_3N_6$ in Figure 4a indicates a pronounced electron localization along the one-dimensional (1D) channels, while this feature is not shown in either Rb_6O nor Rb_9O_2. Structurally, *Cmcm* $Li_2Ca_3N_6$ is also analogical to Mn_5Si_3-type structures ($P6_3/mcm$, no. 193). Interestingly, a few A_5B_3 compounds belonging to the same structural prototype have been identified as electride phases recently.[16,17] In particular, $Li_2Ca_3N_6$ contains very similar chemical entities to that in Sr_5P_3,[17] in which two different sites of Sr atoms correspond to Li and Ca in $Li_2Ca_3N_6$. Similar to Sr_5P_3, there exist large channels with average radii of 2.58 Å along the *c* axis at both the center and corner of the unit cell, which coincide with the ELF basin as depicted in Figure 4a. To check if these channels can accommodate the extra electrons, we further computed the partial charge density at $E_{Fermi} \pm 0.025$ eV (Figure 4b). Clearly, the DOS primarily accumulates around the $[N_2]$ units and the 1D channels. Therefore, we confirm that $Li_2Ca_3N_6$ is a 1D-like electride, like those Mn_5Si_3-type electrides (Y_5Si_3,[16] Sr_5P_3,[17] Yb_5Sb_3[20]).

Each chemical formula Sr_5P_3 has one extra unit of charge, while each $Li_2Ca_3[N_2]_3$ has two if we assign $[N_2]$ to the -II valence state. This means that each 1D channel in $Li_2Ca_3[N_2]_3$ should have twice of the charge density of that in Sr_5P_3. Indeed, our Bader charge analysis supported this scenario. Between the range of $-1.5 < E - E_{Fermi} < 0$ eV, the integrated interstitial electrons is 1.119*e* (see details in Table 2 and Figure 5c,d), which is nearly twice of the reported values (0.594*e*−0.617*e*) in Sr_5P_3.[17] As such, we conclude that $Li_2Ca_3N_6$ is an electride with a formula of $Li_2Ca_3[N_2]_3^{2-}{:}2e^-$, as opposed to its A_5B_3 analogue $Sr_5P_3{:}e^-$.

Interplay between $[N_2]$ and Interstitial Electrons. The discovery of two new electrides suggests a new class of inorganic electrides with the presence of a $[N_2]$ unit. These compounds can exist in crystals with at least two characteristic cavities (1D channel and 2D layer). Such kind of materials may be neglected at the first step of screening if one looks into the total formal charge only by the chemical formula. N atoms usually exhibit two positive valence states: -III (NH_3) and -II (N_2O_4), but the cases of $[N_2]^{2-}$ and $[N_2]^{3-}$ are generally ignored. The presence of $[N_2]$ also makes BaN and $Li_2Ca_3N_6$ different from those previously identified electrides such as 2D-Ca_2N and 1D-Sr_5P_3. In those electrides, the DOS near E_{Fermi} is

DOI: 10.1021/acsami.8b18676
ACS Appl. Mater. Interfaces XXXX, XXX, XXX−XXX

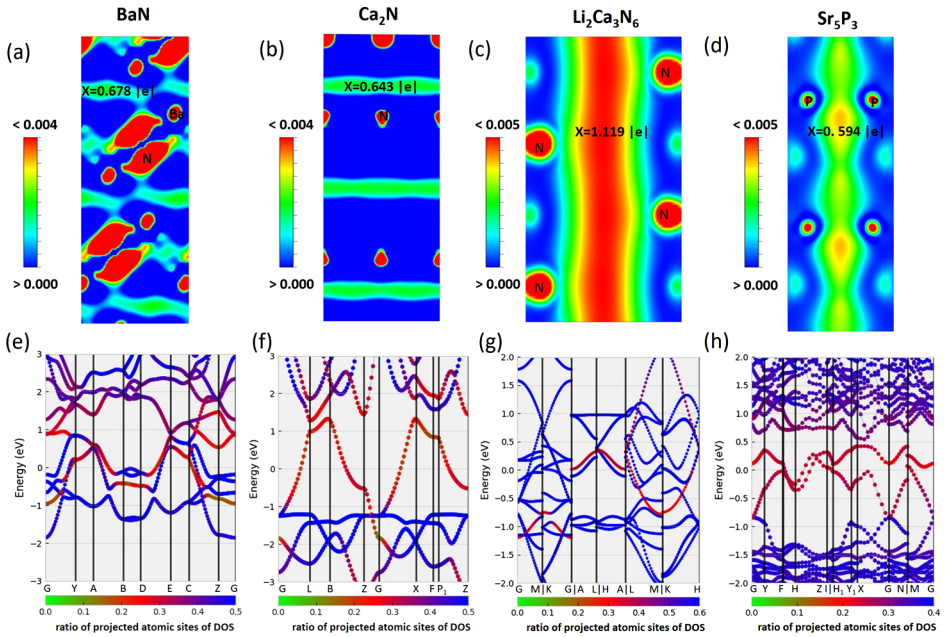

Figure 5. Partial charge density maps of BaN (a) at (010) plane, Ca_2N (b) at (100) plane, $Li_2Ca_3N_6$ (c) at (010) plane, and Sr_5P_3 (d) at (1−10) plane around the Fermi level (-1 eV < $E - E_{Fermi}$ < 0 eV); (e−h) represent the corresponding band structures. The contribution of atoms to each state is shown in figures; the color of dots indicates the weight of all the atoms to the states in the unit cell. Wigner−Seitz radii of Li, Ca, N, Ba, Sr, and P are set to be 1.38, 1.75, 0.74, 1.98, 2.14, and 1.23 Å, respectively, which are consistent with the values in the corresponding POTCAR files used in the VASP code.

mainly contributed by the interstitial electrons.[9,17] However, as shown in Figures 2 and 4, both BaN and $Li_2Ca_3N_6$ have significant portions of DOS near the Fermi level because of the dinitrogen ligands.

To probe the DOS distribution between the electrons localized at $[N_2]$ ligands and the interstitials, we projected the wave function of each energy band onto spherical harmonics that are non-zero within spheres of a radius around each ion. By summing up the spd-wavefunction characters on each ion and the N−N bonding centers, we obtained the contribution of each *K* point on each band. If all electrons are fully localized around the nucleus or the covalent bond path maximum, the sum should be close to 1. Because of the choice of the Wigner−Seitz radius, one usually obtains some values between 0.5 and 1.0 for the bands with large dispersion. On the other hand, the ratio close to 0 indicates that the contribution is mainly from the interstitial electrons. Therefore, we plot the colored map for each band for these four electrides. Clearly, the interstitial electrons (shown as red dots) in Ca_2N and Sr_5P_3 form the pure interstitial bands crossing the Fermi level (Figure 5f,h), which is consistent with the previous results.[9,17] However, the bands crossing the Fermi level in BaN and $Li_2Ca_3N_6$ show a mixture of two different fragments from interstitial electrons (red) and N−N bonding (blue), as shown in Figure 5e,g. Considering that these two groups of electrons will have different electronic activities, we expect the different arrangements will lead to a marked anisotropic effect on the macroscopic properties like mobility and work function. As such, it may provide a route to make novel functional electride materials with desired anisotropy.

On the other hand, the distribution of interstitial electrons also depends on the electronegativity of the $[N_2]$ entity. Although the $[N_2]$ units in BaN and $Li_2Ca_3N_6$ have close N−N bond length, they exhibit different valence states because of different coordination environments. This suggests a possibility to modulate the concentration of interstitial electrons without changing the chemical stoichiometry. Furthermore, such materials are likely to be extended to other systems which contain other ligands like $[C_2]$ and $[O_2]$. Many polyatomic anions species (such as $[I_3]^-$, $[O_2]^{2-}$, $[C_2]^{2-}$) occur frequently in the inorganic compounds, suggesting a viable opportunity to make electrides based on them. Indeed, we mention that a similar compound Ca_2C with $[C_2]$ was predicted to be an electride recently.[24] Unlike the traditional electrides without polyatomic anions, the presence of $[C_2]/[N_2]$ can substantially change the DOS distribution of interstitial electrons and the electronic band structure. As such, it may provide a new route for the design of novel electride materials.

CONCLUSIONS

In summary, we combined a high-throughput screening method with ab initio evolutionary structure search to explore electrides with $[N_2]$ units within both binary and ternary systems. From first-principles CSP, we predicted a marginally stable binary compound BaN as a layered electride. This is the first example of an inorganic electride with pure $[N_2]$ units to our best knowledge. We further performed a systematic investigation on the existing materials and found that another ternary compound $Li_2Ca_3N_6$ also contains both $[N_2]$ and interstitial electrons. Though $Li_2Ca_3N_6$ has been synthesized in the past, its electride nature has not been discovered until our newly developed screening strategy. The presence of $[N_2]$ may substantially change the DOS distribution of interstitial electrons and the electronic band structure and thus may provide a route to improve the functionality of electride materials in the future.

DOI: 10.1021/acsami.8b18676
ACS Appl. Mater. Interfaces XXXX, XXX, XXX−XXX

■ ASSOCIATED CONTENT

Supporting Information

The Supporting Information is available free of charge on the ACS Publications website at DOI: 10.1021/acsami.8b18676.

Structure details of compounds (CIF)

Comparison of low-energy structures in the Ba−N system found in the current work and reference and structural information in VASP's POSCAR format (PDF)

■ AUTHOR INFORMATION

Corresponding Authors

*E-mail: 06010@cau.edu.cn (W.Z.).
*E-mail: qiang.zhu@unlv.edu (Q.Z.).

ORCID

Shengcai Zhu: 0000-0003-3311-6723
Qiang Zhu: 0000-0002-9892-0344

Notes

The authors declare no competing financial interest.

■ ACKNOWLEDGMENTS

Work at UNLV is supported by the National Nuclear Security Administration under the Stewardship Science Academic Alliances program through DOE Cooperative Agreement DE-NA0001982. This work is also supported by the National High Technology Research and Development Program of China (863 program) with grant no. 2015AA034201. We also acknowledge the supports from NSFC (grant nos. 21703004, 61474142, and 11474355) and from China scholarship council (no. 201706350087). The computing resources are provided by XSEDE (TG-DMR180040) and the Center for Functional Nanomaterials under contract no. DE-AC02-98CH10086.

■ REFERENCES

(1) Dye, J. L. Electrides: Early Examples of Quantum Confinement. *Acc. Chem. Res.* **2009**, *42*, 1564−1572.

(2) Li, Z.; Yang, J.; Hou, J. G.; Zhu, Q. Inorganic Electrides. *Chem.—Eur. J.* **2004**, *10*, 1592−1596.

(3) Dawes, S. B.; Ward, D. L.; Huang, R. H.; Dye, J. L. First Electride Crystal Structure. *J. Am. Chem. Soc.* **1986**, *108*, 3534−3535.

(4) Matsuishi, S.; Toda, Y.; Miyakawa, M.; Hayashi, K.; Kamiya, T.; Hirano, M.; Tanaka, I.; Hosono, H. High-density Electron Anions in a Nanoporous Single Crystal: $[Ca_{24}Al_{28}O_{64}]^{4+}(4e^-)$. *Science* **2003**, *301*, 626−629.

(5) Kitano, M.; Inoue, Y.; Yamazaki, Y.; Hayashi, F.; Kanbara, S.; Matsuishi, S.; Yokoyama, T.; Kim, S.-W.; Hara, M.; Hosono, H. Ammonia Synthesis Using a Stable Electride as an Electron Donor and Reversible Hydrogen Store. *Nat. Chem.* **2012**, *4*, 934.

(6) Kanbara, S.; Kitano, M.; Inoue, Y.; Yokoyama, T.; Hara, M.; Hosono, H. Mechanism Switching of Ammonia Synthesis Over Ru-Loaded Electride Catalyst at Metal-Insulator Transition. *J. Am. Chem. Soc.* **2015**, *137*, 14517−14524.

(7) Kim, S. W.; Toda, Y.; Hayashi, K.; Hirano, M.; Hosono, H. Synthesis of a Room Temperature Stable $12CaO{\cdot}7Al_2O_3$ Electride from the Melt and Its Application as an Electron Field Emitter. *Chem. Mater.* **2006**, *18*, 1938−1944.

(8) Keve, E. T.; Skapski, A. C. Ca_2N: a Nitride with a Layer Structure. *Chem. Commun.* **1966**, 829−830.

(9) Lee, K.; Kim, S. W.; Toda, Y.; Matsuishi, S.; Hosono, H. Dicalcium Nitride as a Two-dimensional Electride with an Anionic Electron Layer. *Nature* **2013**, *494*, 336.

(10) Menamparambath, M. M.; Park, J.-H.; Yoo, H.-S.; Patole, S. P.; Yoo, J.-B.; Kim, S. W.; Baik, S. Large Work Function Difference Driven Electron Transfer from Electrides to Single-walled Carbon Nanotubes. *Nanoscale* **2014**, *6*, 8844.

(11) Zhao, S.; Li, Z.; Yang, J. Obtaining Two-Dimensional Electron Gas in Free Space without Resorting to Electron Doping: an Electride Based Design. *J. Am. Chem. Soc.* **2014**, *136*, 13313−13318.

(12) Hu, J.; Xu, B.; Yang, S. A.; Guan, S.; Ouyang, C.; Yao, Y. 2D Electrides as Promising Anode Materials for Na-Ion Batteries from First-Principles Study. *ACS Appl. Mater. Interfaces* **2015**, *7*, 24016−24022.

(13) Uijttewaal, M. A.; de Wijs, G. A.; de Groot, R. A. Low Work Function of the (1000) Ca_2N Surface. *J. Appl. Phys.* **2004**, *96*, 1751−1753.

(14) Guan, S.; Huang, S. Y.; Yao, Y.; Yang, S. A. Tunable Hyperbolic Dispersion and Negative Refraction in Natural Electride Materials. *Phys. Rev. B* **2017**, *95*, 165436.

(15) Zhang, X.; Xiao, Z.; Lei, H.; Toda, Y.; Matsuishi, S.; Kamiya, T.; Ueda, S.; Hosono, H. Two-Dimensional Transition-Metal Electride Y_2C. *Chem. Mater.* **2014**, *26*, 6638−6643.

(16) Lu, Y.; Li, J.; Tada, T.; Toda, Y.; Ueda, S.; Yokoyama, T.; Kitano, M.; Hosono, H. Water Durable Electride Y_5Si_3 : Electronic Structure and Catalytic Activity for Ammonia Synthesis. *J. Am. Chem. Soc.* **2016**, *138*, 3970−3973.

(17) Wang, J.; Hanzawa, K.; Hiramatsu, H.; Kim, J.; Umezawa, N.; Iwanaka, K.; Tada, T.; Hosono, H. Exploration of Stable Strontium Phosphide-Based Electrides: Theoretical Structure Prediction and Experimental Validation. *J. Am. Chem. Soc.* **2017**, *139*, 15668−15680.

(18) Wu, J.; Gong, Y.; Inoshita, T.; Fredrickson, D. C.; Wang, J.; Lu, Y.; Kitano, M.; Hosono, H. Tiered Electron Anions in Multiple Voids of LaScSi and Their Applications to Ammonia Synthesis. *Adv. Mater.* **2017**, *29*, 1700924.

(19) Park, J.; Lee, K.; Lee, S. Y.; Nandadasa, C. N.; Kim, S.; Lee, K. H.; Lee, Y. H.; Hosono, H.; Kim, S.-G.; Kim, S. W. Strong localization of Anionic Electrons at Interlayer for Electrical and Magnetic Anisotropy in Two-dimensional Y_2C Electride. *J. Am. Chem. Soc.* **2017**, *139*, 615−618.

(20) Lu, Y.; Wang, J.; Li, J.; Wu, J.; Kanno, S.; Tada, T.; Hosono, H. Realization of Mott-insulating Electrides in Dimorphic Yb_5Sb_3. *Phys. Rev. B* **2018**, *98*, 125128.

(21) Tada, T.; Takemoto, S.; Matsuishi, S.; Hosono, H. High-Throughput ab Initio Screening for Two-Dimensional Electride Materials. *Inorg. Chem.* **2014**, *53*, 10347−10358.

(22) Inoshita, T.; Jeong, S.; Hamada, N.; Hosono, H. Exploration for Two-Dimensional Electrides via Database Screening and Ab-Initio Calculation. *Phys. Rev. X* **2014**, *4*, 031023.

(23) Ming, W.; Yoon, M.; Du, M.-H.; Lee, K.; Kim, S. W. First-Principles Prediction of Thermodynamically Stable Two-Dimensional Electrides. *J. Am. Chem. Soc.* **2016**, *138*, 15336−15344.

(24) Zhang, Y.; Wang, H.; Wang, Y.; Zhang, L.; Ma, Y. Computer-Assisted Inverse Design of Inorganic Electrides. *Phys. Rev. X* **2017**, *7*, 011017.

(25) Zhao, S.; Kan, E.; Li, Z. Electride: from Computational Characterization to Theoretical Design. *Wiley Interdiscip. Rev.: Comput. Mol. Sci.* **2016**, *6*, 430−440.

(26) Burton, L. A.; Ricci, F.; Chen, W.; Rignanese, G.-M.; Hautier, G. High-Throughput Identification of Electrides from All Known Inorganic Materials. *Chem. Mater.* **2018**, *30*, 7521−7526.

(27) Jain, A.; Ong, S. P.; Hautier, G.; Chen, W.; Richards, W. D.; Dacek, S.; Cholia, S.; Gunter, D.; Skinner, D.; Ceder, G.; Persson, K. A. Commentary: The Materials Project: A materials Genome Approach to Accelerating Materials innovation. *APL Mater.* **2013**, *1*, 011002.

(28) Oganov, A. R.; Glass, C. W. Crystal Structure Prediction Using ab initio Evolutionary Techniques: Principles and Applications. *J. Chem. Phys.* **2006**, *124*, 244704.

(29) Lyakhov, A. O.; Oganov, A. R.; Stokes, H. T.; Zhu, Q. New Developments in Evolutionary Structure Prediction Algorithm USPEX. *Comput. Phys. Commun.* **2013**, *184*, 1172−1182.

DOI: 10.1021/acsami.8b18676
ACS Appl. Mater. Interfaces XXXX, XXX, XXX−XXX

(30) Zhu, S.-c.; Wang, L.; Qu, J.-y.; Wang, J.-j.; Frolov, T.; Chen, X.-Q.; Zhu, Q. Computational Design of Flexible Electrides with Non-trivial Band Topology. **2018**, ArXiv e-prints, arXiv:1811.11334.
(31) Oganov, A. R.; Lyakhov, A. O.; Valle, M. How Evolutionary Crystal Structure Prediction Works-and Why. *Acc. Chem. Res.* **2011**, *44*, 227−237.
(32) Blöchl, P. E. Projector Augmented-wave Method. *Phys. Rev. B: Condens. Matter Mater. Phys.* **1994**, *50*, 17953.
(33) Kresse, G.; Furthmüller, J. Efficient Iterative Schemes for ab initio Total-energy Calculations Using a Plane-wave Basis Set. *Phys. Rev. B: Condens. Matter Mater. Phys.* **1996**, *54*, 11169−11186.
(34) Perdew, J. P.; Burke, K.; Ernzerhof, M. Generalized Gradient Approximation Made Simple. *Phys. Rev. Lett.* **1996**, *77*, 3865−3868.
(35) Klimeš, J.; Bowler, D. R.; Michaelides, A. Van der Waals Density Functionals Applied to Solids. *Phys. Rev. B: Condens. Matter Mater. Phys.* **2011**, *83*, 195131.
(36) Togo, A.; Oba, F.; Tanaka, I. First-principles Calculations of the Ferroelastic Transition between Rutile-type and $CaCl_2$-type SiO_2 at High Pressures. *Phys. Rev. B: Condens. Matter Mater. Phys.* **2008**, *78*, 134106.
(37) Setyawan, W.; Curtarolo, S. High-throughput Electronic Band Structure Calculations: Challenges and Tools. *Comput. Mater. Sci.* **2010**, *49*, 299−312.
(38) Bader, R. F. W. *Atoms in Molecules—A Quantum Theory*; Oxford University Press, 1990.
(39) Steinbrenner, U.; Simon, A. Ba_3N−a New Binary Nitride of an Alkaline Earth Metal. *Z. Anorg. Allg. Chem.* **1998**, *624*, 228−232.
(40) Reckeweg, O.; DiSalvo, F. Crystal Structure of Dibarium Mononitride, Ba_2N, an Alkaline Earth Metal Subnitride. *Z. Kristallogr.—New Cryst. Struct.* **2005**, *220*, 549−550.
(41) Choi, C. S. Neutron Diffraction Study of $Ba(N_3)_2$. *Acta Crystallogr., Sect. B: Struct. Crystallogr. Cryst. Chem.* **1969**, *25*, 2638−2644.
(42) Reckeweg, O.; Simon, A. Azide und Cyanamide - ähnlich und doch anders/Azides and Cyanamides - Similar and Yet Different. *Z. Naturforsch., B: J. Chem. Sci.* **2003**, *58*, 1097−1104.
(43) Vajenine, G. V.; Auffermann, G.; Prots, Y.; Schnelle, W.; Kremer, R. K.; Simon, A.; Kniep, R. Preparation, Crystal Structure, and Properties of Barium Pernitride, BaN_2. *Inorg. Chem.* **2001**, *40*, 4866−4870.
(44) Walsh, A.; Scanlon, D. O. Electron Excess in Alkaline Earth Sub-nitrides: 2D Electron Gas or 3D Electride? *J. Mater. Chem. C* **2013**, *1*, 3525−3528.
(45) Huang, B.; Frapper, G. Barium-Nitrogen Phases Under Pressure: Emergence of Structural Diversity and Nitrogen-Rich Compounds. *Chem. Mater.* **2018**, *30*, 7623−−7636.
(46) MacKay, B. A.; Fryzuk, M. D. Dinitrogen Coordination Chemistry: On the Biomimetic Borderlands. *Chem. Rev.* **2004**, *104*, 385−402.
(47) Evans, W. J.; Lee, D. S.; Rego, D. B.; Perotti, J. M.; Kozimor, S. A.; Moore, E. K.; Ziller, J. W. Expanding Dinitrogen Reduction Chemistry to Trivalent Lanthanides via the LnZ_3/Alkali Metal Reduction System: Evaluation of the Generality of Forming $Ln_2(\mu\text{-}\eta^2\text{:}\eta^2\text{-}N_2)$ Complexes via LnZ_3/K. *J. Am. Chem. Soc.* **2004**, *126*, 14574−14582.
(48) Jaroschik, F.; Momin, A.; Nief, F.; Le Goff, X.-F.; Deacon, G. B.; Junk, P. C. Dinitrogen Reduction and C-H Activation by the Divalent Organoneodymium Complex $[(C_5H_2tBu_3)2Nd(\mu I)K([18]\text{-crown6})]$. *Angew. Chem., Int. Ed.* **2009**, *48*, 1117−1121.
(49) Evans, W. J.; Fang, M.; Zucchi, G.; Furche, F.; Ziller, J. W.; Hoekstra, R. M.; Zink, J. I. Isolation of Dysprosium and Yttrium Complexes of a Three-Electron Reduction Product in the Activation of Dinitrogen, the $(N_2)^{3-}$ Radical. *J. Am. Chem. Soc.* **2009**, *131*, 11195−11202.
(50) Henkelman, G.; Arnaldsson, A.; Jónsson, H. A Fast and Robust Algorithm for Bader Decomposition of Charge Density. *Comput. Mater. Sci.* **2006**, *36*, 354−360.
(51) Schneider, S. B.; Frankovsky, R.; Schnick, W. Synthesis of Alkaline Earth Diazenides $M_{AE}N_2$(M_{AE} = Ca, Sr, Ba) by Controlled Thermal Decomposition of Azides under High Pressure. *Inorg. Chem.* **2012**, *51*, 2366−2373.
(52) Schneider, S. B.; Seibald, M.; Deringer, V. L.; Stoffel, R. P.; Frankovsky, R.; Friederichs, G. M.; Laqua, H.; Duppel, V.; Jeschke, G.; Dronskowski, R.; Schnick, W. High-Pressure Synthesis and Characterization of $Li_2Ca_3[N_2]_3$: An Uncommon Metallic Diazenide with $[N_2]^{2-}$ Ions. *J. Am. Chem. Soc.* **2013**, *135*, 16668−16679.

DOI: 10.1021/acsami.8b18676
ACS Appl. Mater. Interfaces XXXX, XXX, XXX−XXX